J. Fluid Mech. (2004), *vol.* 504, *pp.* 41–60.
DOI: 10.1017/S002211200400816X Printed in the United Kingdom

Macroscale model and viscous–inertia effects for Navier–Stokes flow in a radial fracture with corrugated walls

By M. BUÈS, M. PANFILOV, S. CROSNIER AND C. OLTEAN

Laboratoire Environnement, Géomécanique et Ouvrages – LAEGO – ENSG – INPL Rue du Doyen Marcel Roubault, BP 40, 54501 Vandoeuvre-lès-Nancy, France
michel.bues@ensg.inpl-nancy.fr

(Received 14 February 2003 and in revised form 6 October 2003)

The radial Navier–Stokes flow in a fracture bounded by impermeable corrugated rock surfaces is significantly different from the commonly used creeping flow model between two parallel surfaces, described by Darcy's law on the macroscale. Continuous variations in the Reynolds number along the radial coordinate determine the important role of the nonlinear inertial effects, which are reinforced by local oscillations of the velocity field caused by wall corrugation. The system behaviour is studied both analytically and numerically. A solution for the full system of Navier–Stokes equations in a thin cylindrical domain with oscillating walls is developed as a biparametric and two-scale asymptotic expansion with respect to fracture aperture and corrugation period. The numerical solution is derived based on the finite volume method. A new macroscale flow equation is obtained, which explicitly displays the relative roles of viscous dissipation caused by corrugation, local and global inertia, and cross inertia–viscous effects. The effective flow parameters are defined using analytical relationships.

1. Introduction

Various problems in hydrogeology, petroleum engineering and underground waste deposits concern radial flow through a thin fracture. The most important scientific problem here consists in studying the effective properties of the flow.

At first glance, the examined flow would seem to be very similar to two cases that have been studied in depth in the literature. These are the plane-parallel flow between two parallel plates, and the radial flow in a two-dimension diverging/converging cone with a rather small angle of aperture (Savage 1963; Iwai 1976; Landau & Lifshitz 1986; Zimmerman & Bodvarsson 1996). However, this similarity is only apparent.

Two basic phenomena significantly differentiate the radial flow in a cylindrical fracture from other known similar flow cases. First, the variation in the Reynolds number along the radius as far as to infinity at the fracture centre requires that we use the complete Navier–Stokes system of equations with an important contribution of nonlinear inertia terms. This is in sharp contrast to the plane-parallel flow. On the other hand, this property is similar to that of flow in a diverging/converging cone. However the similarity stops here.

In sharp contrast to the diverging/converging flow which possesses a one-dimensional exact radial solution, purely radial Navier–Stokes flow between two parallel disks does not exist, due to inertia effects, as shown in Peube (1963). Hence

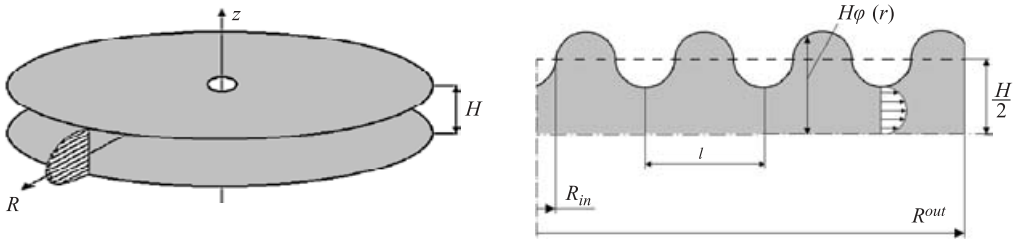

FIGURE 1. Geometry of a corrugated radial fracture.

the flow in such a fracture is always two- or three-dimensional. The continuous flow acceleration directed towards the centre deforms the streamlines by pressing them to the middle plane of the fracture. This leads both to variations in the total viscous dissipation and to the appearance of further two-dimension inertia effects. This *a priori* reasoning means that we may expect the macroscale behaviour of radial flow not to obey Darcy's law. Moreover, it cannot be modelled by the flow in a diverging/converging slot. The existence of wall corrugation will enhance this difference.

The influence of roughness/corrugation in a thin fracture was examined in detail in Adler & Thovert (1999), based on the Stokes equations for plane-parallel flow. Flow in a cylindrical slot was examined only in the case of smooth walls in Peube (1963) where the two-dimensional Navier–Stokes equations were solved in the form of a power series in $1/r$. In Chen (1966) and Crosnier, Chevalier & Buès (2000) experimental data were obtained. The important role of the macroscale inertia effects was confirmed in the recent papers by Vatistas, Ghila & Zitouni (1995) and Zitouni & Vatistas (1997). The effect of inertia upon the flow in a thin fracture was examined in Skjetne, Hansen & Gudmundsson (1999) based on a numerical analysis. The macroscale flow model was not derived as the radial fracture was not the subject of the study. Another common approach to the study of rough fractures consists in detecting empirical corrections to the mean fracture aperture (Iwai 1976; Renshaw 1995).

In this paper the solutions to Navier–Stokes equations and the averaged equation for flow through a radial corrugated fracture are derived based on the asymptotic method. Both the structure of the effective permeability and the nonlinear correction to Darcy's law are obtained as functions of the corrugation geometry. Two classes of non-linear terms are distinguished. They are generated both by pure inertia effects and by cross inertia–viscous phenomena. The former are quadratic with respect to velocity, while the latter are cubic. To calculate all the macroscale parameters, the analytical relationships are derived using the analysis of sinusoidal and rectangular corrugations.

2. Formulation of the problem

2.1. *Fracture geometry*

Let (R, θ, Z) be the radial coordinates. Let $\tilde{\varphi} = \tilde{\varphi}(R)$ be the periodic function with period l and with the average equal to 1/2. A fracture is the cylindrical domain $\tilde{F} = \{-H\tilde{\varphi} < Z < H\tilde{\varphi},\ R_{in} < R < R^{out}\}$ shown in figure 1. We assume that $R_{in} > 0$ and $R^{out} < \infty$. A half of this domain will be used, which is designated as $F = \{0 < z < \varphi,\ R_{in}/R^{out} < r < 1\}$ where the following dimensionless variables are introduced:

$r = R/R^{out}$, $z = Z/H$ and $\varphi(r) = \tilde{\varphi}(R)|_{R=rR^{out}}$. If $\varphi = \text{const} = 1/2$ then the fracture walls are two flat disks.

2.2. *Flow equations and boundary conditions*

Let us examine the flow of an incompressible fluid of density ρ and viscosity μ in domain F. For the sake of clarity, the flow is assumed to be directed from the disk centre, i.e. from R_{in} to R^{out}. The anglular component of the flow velocity is assumed to be zero. Hence the two-dimension Navier–Stokes equations are

$$Re\left[v\frac{\partial u}{\partial z} + \omega u\frac{\partial u}{\partial r}\right] = -\frac{\partial p}{\partial r} + \frac{\partial^2 u}{\partial z^2} + \omega^2\frac{1}{r}\frac{\partial}{\partial r}\left(r\frac{\partial u}{\partial r}\right) - \omega^2\frac{u}{r^2}, \tag{2.1a}$$

$$\omega Re\left[v\frac{\partial v}{\partial z} + \omega u\frac{\partial v}{\partial r}\right] = -\frac{\partial p}{\partial z} + \omega\frac{\partial^2 v}{\partial z^2} + \omega^3\frac{1}{r}\frac{\partial}{\partial r}\left(r\frac{\partial v}{\partial r}\right), \tag{2.1b}$$

$$\frac{\partial v}{\partial z} + \omega\frac{1}{r}\frac{\partial(ru)}{\partial r} = 0, \tag{2.1c}$$

where $u = V_r/V^0$, $v = V_z/V^0$, $p = P/P^0$, V^0 is the characteristic flow velocity, and $P^0 = \mu V^0 R^{out}/H^2$ is the characteristic fluid pressure.

Four dimensionless parameters define the process:

$$\omega = \frac{H}{R^{out}}, \quad \varepsilon = \frac{l}{R^{out}}, \quad Re = \frac{\rho V^0 H}{\mu}, \quad \delta = \frac{R_{in}}{R^{out}}, \tag{2.2}$$

where Re is the Reynolds number. Usually, the flow rate, Q, is known instead of the characteristic velocity. Then velocity V^0 can be specified as $V^0 = Q/(2\pi H R^{out})$.

In this paper we develop a family of solutions, which correspond to no-slip conditions at the fracture walls, symmetry conditions at the axis $z = 0$ and the integral condition meaning a fixed flow rate:

$$u|_{z=\varphi} = v|_{z=\varphi} = 0, \quad \left.\frac{\partial u}{\partial z}\right|_{z=0} = v|_{z=0} = 0, \quad \int_0^{\varphi(r)} ru(r,z)\,\mathrm{d}z = \tfrac{1}{2}, \ \forall r. \tag{2.3}$$

The last condition, being satisfied at a fixed radius, remains true for all other radii, which follows immediately from the integration of (2.1*c*) over z and taking into account the no-slip conditions.

2.3. *Order of parameters and corrugation classes*

The fracture aperture is assumed to be small with respect to the fracture radius: $0 < \omega \ll 1$. The Reynolds number is not limited, but the flow is assumed to be always stable. More strictly speaking, we will assume that the turbulent zone is always located outside domain F, at $R < R_{in}$. This imposes certain limits upon the simultaneous values of parameters Re and δ, such that the following must hold: $\delta > Re/Re_{cr}$, where Re_{cr} is the critical Reynolds number marking the transition to turbulence. This inequality also gives the upper limit for the Reynolds number at a fixed value of δ.

Parameters ω and ε are responsible for the non-homogeneity of the system along axes z and r respectively. If $\varepsilon \to 0$ then the fracture becomes smooth, hence the velocity and pressure oscillations along r within a period are eliminated. If $\omega \to 0$ then the fracture becomes extremely thin, such that the velocity/pressure variation along z becomes meaningless. Therefore we will call ω and ε the vertical and the horizontal heterogeneity scales respectively. Note that the physical origin of these two types of heterogeneity is different: vertical heterogeneity (of flow velocity) is caused

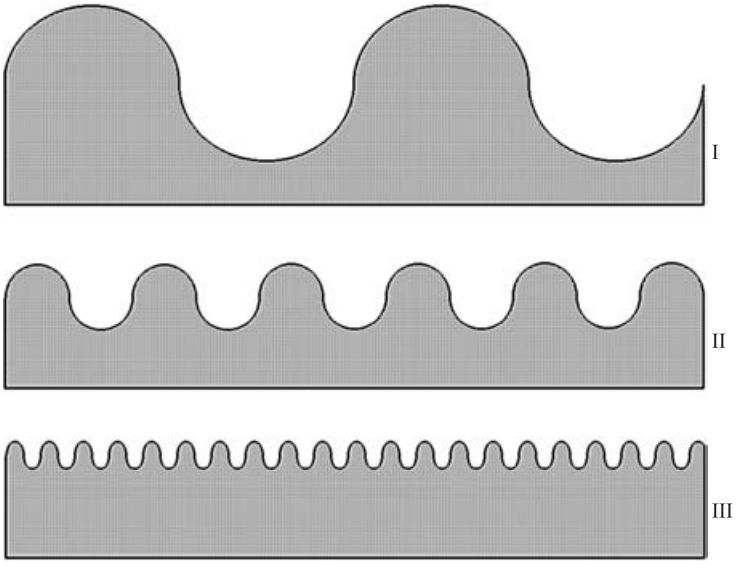

FIGURE 2. Classes of corrugation.

by the different degree of friction between the domain in the vicinity of the walls and in the flow centre. This kind of velocity heterogeneity does not entail any flow acceleration along z. Horizontal heterogeneity is caused by the spatial oscillations of the pore walls. This kind of heterogeneity gives rise to acceleration/deceleration and inertia effects.

The macroscale, non-oscillating, behaviour is then obtained by a double integration of the system along z over the entire height H (vertical homogenization) and along r over one corrugation period l (horizontal homogenization).

Three distinct corrugation classes may be selected depending on the ratio between parameters ω and ε (figure 2):

$$\text{I – rare corrugation:}\quad \omega \ll \varepsilon \ll 1; \tag{2.4a}$$

$$\text{II – frequent corrugation:}\quad \omega \sim \varepsilon; \tag{2.4b}$$

$$\text{III – fine-scale corrugation:}\quad \varepsilon \ll \omega. \tag{2.4c}$$

It is obvious that in the third case corrugation plays a local role and cannot influence the flow structure overall. This case has been studied in Skjetne *et al.* (1999) for plan-parallel flow.

In the first and second cases, corrugation could modify the entire flow structure. The first case is preferable for the analysis, as the vertical and horizontal heterogeneity scales are separate (i.e. very different). This enables the homogenization procedures along z and along r to be separated, which becomes a powerful tool for theoretical analysis. In the present paper, only the first case has been studied.

The corrugation amplitude is always limited by construction, so that $\min(\varphi) > 0$. Moreover, we will assume that the corrugation amplitude is no higher than the corrugation period: $H(\max(\varphi) - \min(\varphi)) \leqslant l$. Using (2.2), we obtain $(\max(\varphi) - \min(\varphi)) \leqslant \varepsilon/\omega$. Otherwise, the corrugation amplitude should be examined as an additional large parameter which could significantly modify the asymptotic expansion structure.

3. Methods of solution

The method of solution consists in developing the asymptotic expansions at $\omega \to 0$ and $\varepsilon \to 0$. At limit $\varepsilon \to 0$ we will obtain a system that is homogenized along r. The limit $\omega \to 0$ formally means elimination of the vertical variable z, which is close to homogenization along z. Thus the zero term of the asymptotic expansion is expected to be equal to an averaged value or to be close to it in some way. Hence the asymptotic solution method is close to homogenization. Owing to the particularity of the method used, the solutions obtained do not need to provide an exact detailed flow pattern, but they are expected to exhibit adequate homogenized behaviour.

For case I in (2.4*a*), when the heterogeneity scales are separated, asymptotic expansion can be performed in two consecutive steps.

3.1. *Asymptotic expansions as* $\omega \to 0$

In the first step, the parameter ε is considered as fixed and the solution to problem (2.1)–(2.3) is constructed as a regular asymptotic expansion at $\omega \to 0$:

$$\left.\begin{aligned} u(r, z; \omega) &= u_0(r, z) + \omega u_1(r, z) + \omega^2 \ldots, \\ v(r, z; \omega) &= v_0(r, z) + \omega v_1(r, z) + \omega^2 \ldots, \\ p(r, z; \omega) &= p_0(r, z) + \omega p_1(r, z) + \omega^2 \ldots. \end{aligned}\right\} \tag{3.1}$$

As is usual for certain thin structures, such an asymptotic expansion should, in the zero term, lead to functions averaged over the fracture aperture, or, at least, to functions whose behaviour along z corresponds to the exact solution in the average sense only.

Strictly speaking, (2.1) are singularly perturbed with respect to parameter ω. When $\omega = 0$, the highest derivatives with respect to r are lost. This may be a cause of boundary layer phenomena in the vicinity of the inlet or the outlet section of the domain. Within the framework of our analysis, when the boundary conditions at the inlet and the outlet are not examined, boundary layer effects may be neglected. However, it must not be forgotten that this assumption reduces the family of constructed solutions.

3.2. *Asymptotic expansion as* $\varepsilon \to 0$ *and homogenization*

The second step of the method consists in developing an ε-expansion. The expansion obtained in previous sections will contain fast oscillating functions along r with a small period ε. The expansion over ε should be performed in terms of a two-scale asymptotic expansion. Instead of any function $f(r, r/\varepsilon, z)$ we introduce a 'two-scale function' $\tilde{f}(r, y, z)$, such that $\tilde{f}(r, y, z)|_{y=r/\varepsilon} = f(r, r/\varepsilon, z)$, where y is the new 'fast' variable. Hence, for the derivative we obtain

$$\frac{\partial f}{\partial r} = \frac{\partial \tilde{f}}{\partial r} + \frac{1}{\varepsilon}\frac{\partial \tilde{f}}{\partial y}.$$

Such a two-scale asymptotic expansion is equivalent to a homogenization procedure. In the case examined, when homogenization is not applied to a differential equation but to an algebraic series, the homogenization procedure over ε is reduced to two steps: (*a*) a reordering of the terms in the expansion at $\omega \to 0$, and (*b*) an integration of this series over the fast variable y. This integration represents the averaging over corrugations. We will also apply a second averaging, over the fracture aperture to a flow through a narrow slot.

The full homogenized model can then be obtained by a double homogenization both over the fracture aperture and over the radial wall corrugations. The homogenization

over corrugations and double averaging for a two-scale function $\tilde{f}(r, y, z)$ are defined as

$$\langle f \rangle = \int_0^1 \tilde{f}(r, y, z)\, \mathrm{d}y, \qquad \langle\langle f \rangle\rangle = \int_0^1 \left(\frac{1}{\varphi} \int_0^{\varphi} \tilde{f}(r, y, z)\, \mathrm{d}z \right) \mathrm{d}y. \tag{3.2}$$

3.3. *Numerical method*

Simulations were carried out with the CFD-ACE package based on the finite volume method. Structured Cartesian grids were generated. The grid refinement selected was 1200–1500 grid cells in the horizontal direction and 20–50 cells in the vertical direction, depending on the corrugation form (sinusoidal or rectangular), when ratio H/R_{out} was of order 0.01. Contrary to the asymptotic method, the numerical analysis requires all the boundary-value conditions to be clearly specified in order to define a single solution. At the fracture inlet, the velocity profile has been defined either as a constant, or as the Poiseuille distribution. A constant pressure distribution was applied at the outlet. A particularly stable first-order numerical scheme was used for the resolution. The SIMPLEC algorithm was used to calculate the pressure–velocity coupling.

4. Asymptotic solution

4.1. *Asymptotic expansions*

Substituting expansion (3.1) into (2.1)–(2.3) we obtain a sequence of boundary-value problems.

In the zero approximation, for u_0, v_0 and p_0 we have

$$\left.\begin{aligned} & Re\, v_0 \frac{\partial u_0}{\partial z} = \frac{\partial p_0}{\partial r} + \frac{\partial^2 u_0}{\partial z^2}, \qquad \frac{\partial p_0}{\partial z} = 0, \qquad \frac{\partial v_0}{\partial z} = 0, \\ & u_0|_{z=\varphi} = 0, \quad v_0|_{z=\varphi} = 0, \quad \left.\frac{\partial u_0}{\partial z}\right|_{z=0} = 0, \quad v_0|_{z=0} = 0, \quad \int_0^{\varphi} r u_0\, \mathrm{d}z = \tfrac{1}{2}. \end{aligned}\right\} \tag{4.1}$$

This gives immediately $v_0 \equiv 0$.

In the first approximation, for u_1, v_1 and p_1 we have

$$\left.\begin{aligned} & Re \left[v_1 \frac{\partial u_0}{\partial z} + u_0 \frac{\partial u_0}{\partial r} \right] = -\frac{\partial p_1}{\partial r} + \frac{\partial^2 u_1}{\partial z^2}, \quad \frac{\partial p_1}{\partial z} = 0, \quad \frac{\partial v_1}{\partial z} = -\frac{1}{r} \frac{\partial (r u_0)}{\partial r}, \\ & u_1|_{z=\varphi} = 0, \quad v_1|_{z=\varphi} = 0, \quad \frac{\partial u_1}{\partial z}|_{z=0} = 0, \quad v_1|_{z=0} = 0, \quad \int_0^{\varphi} r u_1\, \mathrm{d}z = 0. \end{aligned}\right\} \tag{4.2}$$

In the second approximation, for u_2, v_2 and p_2 we have

$$\left.\begin{aligned} & Re \left[v_2 \frac{\partial u_0}{\partial z} + v_1 \frac{\partial u_1}{\partial z} + \frac{\partial u_0 u_1}{\partial r} \right] = -\frac{\partial p_2}{\partial r} + \frac{\partial^2 u_2}{\partial z^2} + \frac{1}{r} \frac{\partial}{\partial r} \left(r \frac{\partial u_0}{\partial r} \right) - \frac{u_0}{r^2}, \\ & \frac{\partial p_2}{\partial z} = \frac{\partial^2 v_1}{\partial z^2}, \qquad \frac{\partial v_2}{\partial z} = -\frac{1}{r} \frac{\partial (r u_1)}{\partial r}, \\ & u_2|_{z=\varphi} = 0, \quad v_2|_{z=\varphi} = 0, \quad \frac{\partial u_2}{\partial z}|_{z=0} = 0, \quad v_2|_{z=0} = 0, \quad \int_0^{\varphi} r u_2\, \mathrm{d}z = 0. \end{aligned}\right\} \tag{4.3}$$

4.2. *Analytical solution to the asymptotic problems*

Let us replace variables (r, z) to (r, η) with $\eta = z/\varphi(r)$, such that for any function $f(r, z)$ the following is true:

$$f(r,z) = \tilde{f}(r,\eta)|_{\eta=z/\varphi}, \qquad \frac{\partial f}{\partial r} = \frac{\partial \tilde{f}}{\partial r} - \frac{\eta\varphi_r'}{\varphi}\frac{\partial \tilde{f}}{\partial \eta}, \qquad \frac{\partial f}{\partial z} = \frac{1}{\varphi}\frac{\partial \tilde{f}}{\partial \eta},$$

where $\varphi_r' \equiv \mathrm{d}\varphi/\mathrm{d}r$.

Then all the differential equations in (4.1)–(4.3) may be explicitly integrated. We thus obtain the following analytical solutions:

for problem (4.1)

$$u_0 = -\frac{3}{4r\varphi}(\eta^2 - 1), \qquad v_0 = 0, \qquad \frac{\partial p_0}{\partial r} = -\frac{3}{2r\varphi^3};$$

for problem (4.2)

$$u_1 = -\frac{3Re}{1120}\frac{\Phi_0(r)}{r}(\eta^2-1)(5-28\eta^2+7\eta^4),$$
$$v_1 = \frac{3\varphi_r'}{4r\varphi}(\eta-\eta^3), \quad \frac{\partial p_1}{\partial r} = \frac{27Re}{70}\frac{\Phi_0(r)}{r\varphi^2};$$

for problem (4.3)

$$u_2 = \frac{9Re^2}{4480}\left\{\Phi_1(r)\left[\frac{4111}{2310}(\eta^2-1) - \frac{19}{6}(\eta^4-1) + \frac{34}{15}(\eta^6-1) - \frac{3}{4}(\eta^8-1) + \frac{7}{90}(\eta^{10}-1)\right]\right.$$
$$\left. + \Phi_2(r)\left[-\frac{416}{1155}(\eta^2-1) + \frac{5}{6}(\eta^4-1) - \frac{11}{15}(\eta^6-1) + \frac{1}{4}(\eta^8-1) - \frac{1}{45}(\eta^{10}-1)\right]\right\}$$
$$+ \frac{3}{40}\Phi_3(r)(\eta^2-1)(5\eta^2-1),$$
$$v_2 = -\frac{3Re}{1120}\{\Phi_7(r)[5\eta - 11\eta^3 + 7\eta^5 - \eta^7] - \Phi_8(r)[5\eta - 33\eta^3 + 35\eta^5 - 7\eta^7]\},$$
$$\frac{\partial p_2}{\partial r} = -\frac{3}{5}\Phi_4(r) - \frac{39Re^2}{70\cdot 385}\Phi_5(r) + \frac{3}{4}\Phi_6(r)(1-3\eta^2),$$

where

$$\Phi_0(r) = \frac{\varphi_r'}{r\varphi} + \frac{1}{r^2}, \qquad \Phi_1(r) = \frac{\varphi_{rr}''}{r^3} - \frac{2(\varphi_r')^2}{r^3\varphi} - \frac{4\varphi_r'}{r^4} - \frac{4\varphi}{r^5}, \qquad \Phi_2(r) = \frac{\varphi_{rr}''}{r^3} - \frac{2\varphi}{r^5},$$
$$\Phi_3(r) = \frac{\varphi_{rr}''}{r} - \frac{\varphi_r'}{r^2}, \quad \Phi_4(r) = \frac{\varphi_{rr}''}{r\varphi^2} + \frac{(\varphi_r')^2}{r\varphi^3} - \frac{\varphi_r'}{r^2\varphi^2},$$
$$\Phi_5(r) = \frac{3\varphi_{rr}''}{r^3\varphi^2} - \frac{4(\varphi_r')^2}{r^3\varphi^3} - \frac{8\varphi_r'}{r^4\varphi^2} - \frac{10}{r^5\varphi},$$
$$\Phi_6(r) = \left(\frac{\varphi_r'}{r\varphi^2}\right)', \quad \Phi_7(r) = \frac{(\Phi_0\varphi)'}{r}, \quad \Phi_8(r) = \frac{\Phi_0\varphi'}{r}.$$

4.3. *Asymptotic expansion as* $\varepsilon \to 0$

Let us now examine the expansion obtained in terms of the two-scale functions defined in § 3.2 by introducing a new variable $y = r/\varepsilon$. We wish to underline that the function φ depends on y only, and hence

$$\varphi_r' = \frac{1}{\varepsilon}\varphi_y'.$$

A rearrangement of the series derived in the previous section thus leads to the following final form of the asymptotics at $\omega, \varepsilon \to 0$ for problem (2.1)–(2.3):

$$u = -\frac{3}{4r\varphi}(\eta^2-1) - \frac{3\omega Re}{1120\varepsilon}M_1(\eta)\left(\frac{\varphi'_y}{r^2\varphi} + \varepsilon\frac{1}{r^2} + \varepsilon^2\ldots\right)$$
$$+ \frac{\omega^2}{\varepsilon^2}\left\{\left(\frac{9Re^2}{4480}\left[M_2(\eta)\left(\frac{\varphi''_{yy}}{r^3} - \frac{2(\varphi'_y)^2}{r^3\varphi}\right) + M_3(\eta)\frac{\varphi''_{yy}}{r^3}\right] + \frac{3M_3(\eta)}{40}\frac{\varphi''_{yy}}{r}\right)\right.$$
$$\left. - \varepsilon\left(\frac{9Re^2}{1120}\frac{\varphi'_y}{r^4}M_2(\eta) + \frac{3}{40}\frac{\varphi'_y}{r^2}M_3(\eta)\right) - \varepsilon^2\frac{9Re^2}{2240}\frac{\varphi}{r^5}(2M_2+M_3) + \varepsilon^3\ldots\right\}$$
$$+ O\left(\frac{\omega^3}{\varepsilon^3} + \omega\varepsilon\right), \tag{4.4a}$$

$$v = -\frac{3\omega}{4\varepsilon}(\eta^3-\eta)\frac{\varphi'_y}{r\varphi}$$
$$- \frac{3\omega^2 Re}{1120\varepsilon^2}\left\{\left(M_5(\eta)\frac{\varphi''_{yy}}{r^2} + M_6(\eta)\frac{(\varphi'_y)^2}{r^2\varphi}\right) + \varepsilon\frac{\varphi'_y}{r^3}M_6(\eta) - \varepsilon^2\frac{2\varphi}{r^4}M_5(\eta) + \varepsilon^3\ldots\right\}$$
$$+ O\left(\frac{\omega^3}{\varepsilon^3} + \omega\varepsilon\right), \tag{4.4b}$$

$$\frac{\partial p}{\partial r} = -\frac{3}{2r\varphi^3} + \frac{27\omega Re}{70\varepsilon}\left(\frac{\varphi'_y}{r^2\varphi^3} + \varepsilon\frac{1}{r^3\varphi^2} + \varepsilon^2\ldots\right)$$
$$+ \frac{\omega^2}{\varepsilon^2}\left\{\left[\frac{\varphi''_{yy}}{r\varphi^2}\left(\frac{3}{4}M_7(\eta) - \frac{3}{5} - \frac{39\times 3Re^2}{70\times 385r^2}\right) - \frac{(\varphi'_y)^2}{r\varphi^3}\left(\frac{3}{2}M_7(\eta) + \frac{3}{5} - \frac{39\times 4Re^2}{70\times 385r^2}\right)\right]\right.$$
$$\left. + \varepsilon\frac{\varphi'_y}{r^2\varphi^2}\left[-\frac{3}{4}M_7(\eta) + \frac{3}{5} + \frac{39\times 8Re^2}{70\times 385r^2}\right] + \varepsilon^2\frac{39Re^2}{7\times 385r^5\varphi} + \varepsilon^3\ldots\right\} + O\left(\frac{\omega^3}{\varepsilon^3} + \omega\varepsilon\right), \tag{4.4c}$$

where

$$M_1(\eta) = 7\eta^6 - 35\eta^4 + 33\eta^2 - 5,$$
$$M_2(\eta) = \frac{4111}{2310}(\eta^2-1) - \frac{19}{6}(\eta^4-1) + \frac{34}{15}(\eta^6-1) - \frac{3}{4}(\eta^8-1) + \frac{7}{90}(\eta^{10}-1),$$
$$M_3(\eta) = -\frac{416}{1155}(\eta^2-1) + \frac{5}{6}(\eta^4-1) - \frac{11}{15}(\eta^6-1) + \frac{1}{4}(\eta^8-1) - \frac{1}{45}(\eta^{10}-1),$$
$$M_4(\eta) = 5\eta^4 - 6\eta^2 + 1, \qquad M_5(\eta) = 5\eta - 11\eta^3 + 7\eta^5 - \eta^7,$$
$$M_6(\eta) = -5\eta + 33\eta^3 - 35\eta^5 + 7\eta^7, \qquad M_7(\eta) = 1 - 3\eta^2.$$

The asymptotic solution (4.4) is valid for the following situations: (*a*) $\varepsilon \gg \omega$; (*b*) the function $\varphi(r)$ is doubly differentiable.

4.4. *Stream function*

For a stream function ψ defined as

$$u = -\frac{1}{r}\frac{\partial\psi}{\partial z}, \qquad v = \frac{1}{r}\frac{\partial\psi}{\partial r},$$

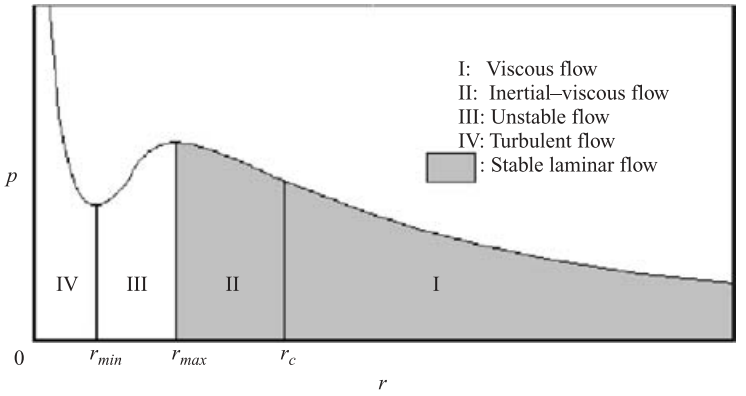

FIGURE 3. Modes of divergent flow through a radial fracture.

the following relationship may be obtained by integration of the first relation with an additional condition $\psi|_{z=\varphi} = 0$:

$$\psi(r,\eta) = \frac{1}{4}(\eta^3 - 3\eta) + \frac{3\omega Re}{1120}\Phi_0\varphi[\eta^7 - 7\eta^5 + 11\eta^3 - 5\eta] - \frac{9\omega^2 Re^2}{4480}\left\{r\varphi\Phi_1\left[\frac{4111}{2310}\left(\frac{\eta^3}{3} - \eta\right) - \frac{19}{6}\left(\frac{\eta^5}{5} - \eta\right) + \frac{34}{5}\left(\frac{\eta^7}{7} - \eta\right) - \frac{3}{4}\left(\frac{\eta^9}{9} - \eta\right) + \frac{7}{90}\left(\frac{\eta^{11}}{11} - \eta\right)\right] + r\varphi\Phi_2\left[-\frac{416}{1155}\left(\frac{\eta^3}{3} - \eta\right) + \frac{5}{6}\left(\frac{\eta^5}{5} - \eta\right) - \frac{11}{15}\left(\frac{\eta^7}{7} - \eta\right) + \frac{1}{4}\left(\frac{\eta^9}{9} - \eta\right) - \frac{1}{45}\left(\frac{\eta^{11}}{11} - \eta\right)\right]\right\} - \frac{3\omega^2}{40}r\varphi\Phi_3(\eta^5 - 2\eta^2 + \eta) + C + O(\omega^3) \quad (4.5)$$

where C is an arbitrary constant.

5. Analysis of the solution for a smooth fracture

5.1. *Qualitative results for a smooth fracture*

For a smooth fracture, when $\varphi = 1/2$, the first approximation at $\omega \to 0$ of asymptotic expansion (4.4) is equivalent to that obtained in Peube (1963), although the latter was derived using a different method (power-value series over $1/r$). Similarly to Peube (1963), the main results following from (4.4) should be noted.

The zero term corresponds to Poiseuille flow. The next terms involve inertia effects. The inertia forces disturb the parabolic velocity profile in such a way that velocity increases in the median plane and decreases in the vicinity of the walls. From a critical radius value, the near-to-wall radial velocity becomes negative, which indicates reverse flow formation.

All the inertia effects disappear when $r \geqslant r_c = \sqrt{\pi\omega Re}$, according to Peube (1963). For a divergent flow directed away from the fracture centre, the pressure along r appears non-monotonic, as seen in figure 3, which illustrates four modes of radial divergent flow. The pressure distribution along r is marked by a local minimum at point r_{min} and a local maximum at point r_{max}, with $r_{min} < r_{max}$. Between these two points the pressure increases along the flow direction. This indicates an unstable

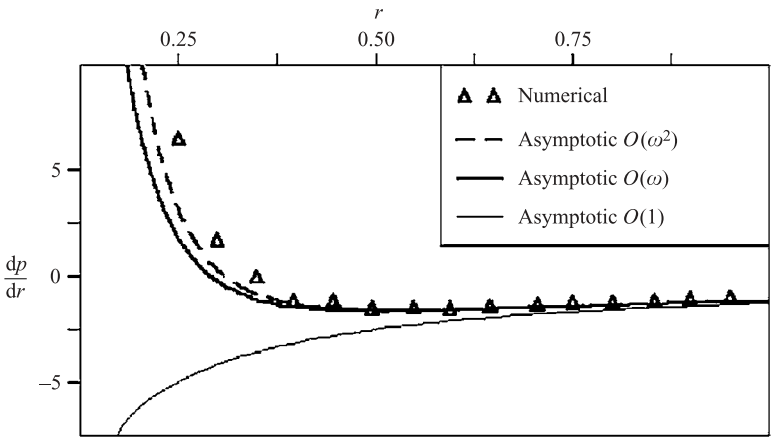

FIGURE 4. Smooth fracture: comparison of numerical and analytical solutions.

process. Hence, any analysis of the stable laminar divergent flow is justified only when $r \geqslant r_{max}$.

The value r_{max} can be estimated from the first approximation of expansion (4.4c). Assuming $\partial p/\partial r = 0$, we obtain

$$r_{max} = 3\sqrt{\frac{\omega Re}{70}} = 0.359\sqrt{\omega Re}.$$

Nevertheless, when the flow is converging, i.e. is directed towards the fracture centre, the zero term in (4.4c) changes sign such that the pressure derivative always remains positive. The pressure distribution is then monotonic and therefore the limitation mentioned above can be ignored.

5.2. *Comparison with a numerical solution for a smooth fracture*

The following parameters have been used for the numerical analysis: $R^{out} = 0.4$ m, $H = 0.008$ m, $R_{in} = 0.01$ m. Numerical results obtained for a smooth fracture are presented in figure 4.

The numerical, Poiseuille and asymptotic theoretical pressure derivatives at the wall are presented in figure 4 for $Re = 66.4$. The best match between the asymptotic solution and the numerical results is observed throughout the stable flow domain, i.e. downstream from r_{max}. The shift of this point towards the outlet section when Re increases is satisfactorily predicted by the solution obtained.

6. Analysis of a corrugated fracture: microscale flow behaviour

The solution obtained can be used both to calculate the microscale flow pattern and to predict the averaged system behaviour.

6.1. *Flow pattern*

The flow pattern has been calculated based on the asymptotic solution (4.4) for a sinusoidal corrugation given by the function

$$\varphi = 0.5\{1 + a\sin(2\pi y)\}, \qquad y = \frac{r}{\varepsilon}, \tag{6.1}$$

with a new dimensionless parameter a equal to the ratio of the corrugation amplitude at half of the mean fracture aperture.

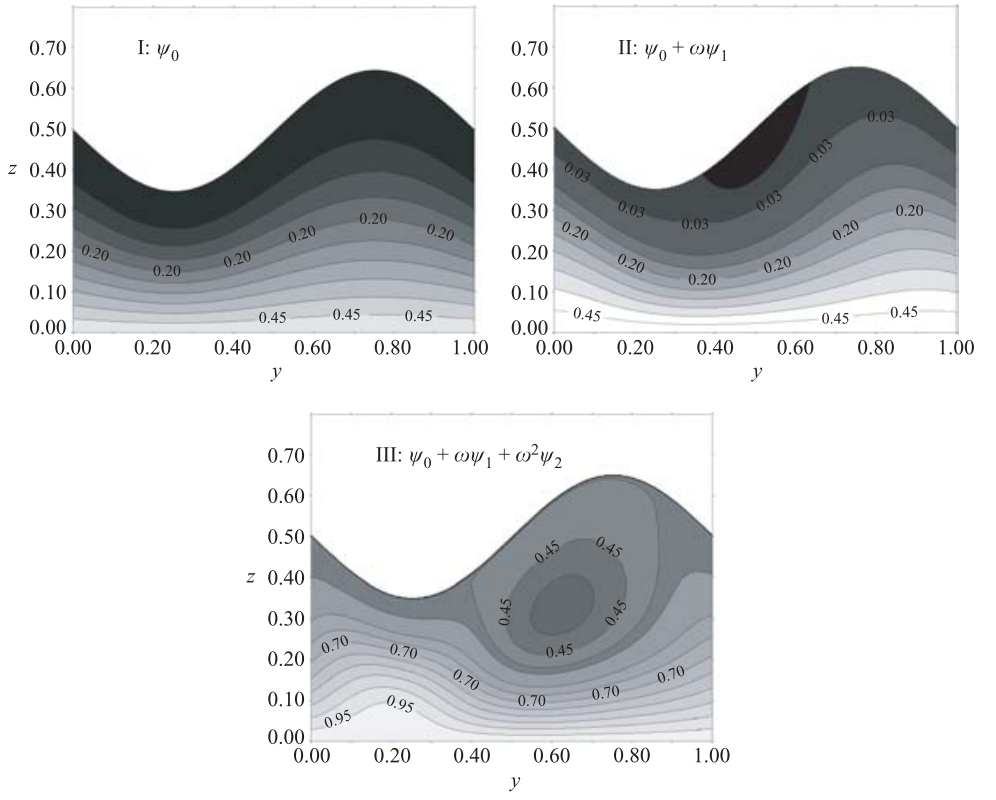

FIGURE 5. Streamlines for a sinusoidal corrugation in the zero (I), first (II) and second (III) approximations of the asymptotic solution.

The stream function has been calculated using (4.5) in the zero, first and second approximations. The results for $Re = 70$, $\omega = 0.01$, $\varepsilon = 0.1$ and $a = 0.3$ are presented in figure 5 in the form of stream-function isolines. The flow travels from left to right, and the upper half-domain is presented. A rather high Reynolds number is chosen in order to ensure the formation of secondary flow. A typical secondary flow is displayed in the form of a vortex formed between the pore wall and the separated stream. The most exact correspondence with the true flow pattern is obtained in the second approximation. The first approximation, although sufficiently sensitive to capture the vortex formation, is nevertheless quantitatively different from the true pattern. The zero approximation, which describes a flow without inertia, always produces a smooth and symmetrical streamline pattern.

6.2. *Criterion for secondary flow formation*

In a fracture with oscillating but smooth walls, flow separation and vortex formation do not necessarily occur even at very high Reynolds numbers, if the wall oscillation amplitude is not sufficiently large. A criterion of vortex formation for a general φ function describing corrugation can be obtained from the analysis of solutions (4.4).

Various approaches may be used to detect when vortex formation or flow separation occurs. In particular, the flow is separated when the normal stress at the wall becomes zero. In Schlichting (1968) the separation instant was associated with the annihilation of the normal derivative of tangential velocity. We will use another approach, enabling us to detect all types of secondary flows, i.e. the near-wall reverse flow described in

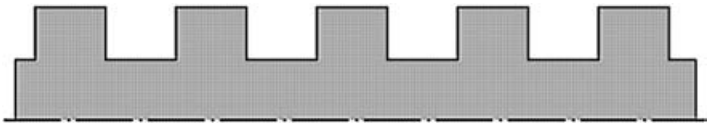

FIGURE 6. Rectangular corrugation.

§ 5.1 and the vortices. It is easy to see that, due to its geometry, the radial vortex always has points at which the velocity vector is strictly vertical. A point with zero horizontal velocity is belongs to a velocity profile which has an inverse flow zone. Both types of secondary flows may be detected by the existence of zero points for the velocity u.

For our purpose, the first approximation is sufficient, because, as has been noted, it is sensitive to vortex formation, as well as to the appearance of reverse flow.

If $u=0$, then relation (4.4a) yields the following equation for η in the first approximation:

$$0=-\frac{3}{4r\varphi}(\eta^2-1)-\frac{3\omega Re}{1120}\frac{\Phi_0(r)}{r}(\eta^2-1)(5-28\eta^2+7\eta^4)$$

or

$$\eta^4-4\eta^2+\left(\frac{5}{7}+\frac{40}{\omega Re\varphi\Phi}\right)=0$$

which has the exact solution:

$$\eta^2=2-\sqrt{\frac{23}{7}-\frac{40}{\omega Re\varphi\Phi}}.$$

The value of η is between 0 and 1. Excluding the wall (which always satisfies the requirement $u=0$, but is of no interest) we obtain the following inequality:

$$0\leqslant 2-\sqrt{\frac{23}{7}-\frac{40}{\omega Re\varphi\Phi}}<1.$$

If $\varphi_r'>0$ then we finally obtain

$$\omega Re\left(\frac{\varphi_r'}{r}+\frac{\varphi}{r^2}\right)>14.$$

A high wall oscillation amplitude and a high Re are favourable to secondary flow formation.

If the fracture is smooth ($\varphi_r'\equiv 0$), we obtain the following criterion for the appearance of a near-wall inverse flow:

$$r<\sqrt{\frac{\omega Re}{28}}=0.189\sqrt{\omega Re}.$$

6.3. *Continuity of the wall surface; rectangular and quasi-rectangular corrugation*

The relationships (3.1) contain the derivatives of the function φ. Hence they are not applicable to discontinuous surfaces. A typical example of such a surface is the rectangular corrugation shown in figure 6 and defined within a single period as

$$\varphi=\begin{cases}1/2-a_1 \text{ when } 0<y\leqslant y^*\\ 1/2+a_2 \text{ when } y^*<y\leqslant 1,\end{cases}\qquad y=r/\varepsilon, \tag{6.2}$$

where $H(a_1+a_2)$ is the amplitude of oscillations and y^* is the relative length of the narrow section within a period. These parameters are related by the formula $a_2 = a_1 y^*/(1-y^*)$, which results from condition $\langle\varphi\rangle = 1/2$.

It is very useful to analyse rectangular corrugation as in many cases it provides the analytical formulae for the macroscale flow parameters.

In order to obtain closed and simple analytical relations for macroscale parameters such as permeability, we introduce a so-called 'quasi-rectangular corrugation'. This type of surface can be obtained from the rectangular surface by eliminating the discontinuity points. This means that in definition (6.2) of the function $\varphi(r)$, non-strict inequalities are replaced by strict inequalities. At the discontinuity points, the function $\varphi(r)$ is not defined. At all the points where the function $\varphi(r)$ is defined, its derivative is zero. In other words, the true fracture with rectangular corrugation is approximately replaced by an artificial combination of two smooth fractures. One of them (the narrowest) has a uniform aperture equal to the minimal aperture of the true fracture, $H(1/2-a_1)$, while the second (the largest) has the maximal aperture $H(1/2+a_2)$. The joints between these two fractures are not defined. This combination of two smooth fractures can be examined as a natural bound of the true corrugated fracture.

Taking into account that the fluid flow across the fracture is basically determined by the narrowest section, it is natural to expect that the true behaviour will be closer to that of the narrowest fracture. Therefore we can *a priori* attempt to improve the representation by using the mean smooth fracture, whose aperture is equal to the mean aperture of the real fracture, instead of the largest fracture.

At the same time, it is clear that the formal elimination of the discontinuity points may seriously modify the streamline pattern in some cases, especially in the case of high inertia effects. The application of the quasi-rectangular model is thus limited and is therefore not recommended at very high Reynolds numbers.

In the next sections we will analyse various examples illustrating to what extent quasi-rectangular corrugation can be used as an approximate model of true undulating fractures.

6.4. *Comparison with a numerical solution for a corrugated fracture*

The example of a rectangular corrugation was selected to compare the solutions obtained with those from numerical data. The analytical data have been obtained for the quasi-rectangular corrugation described above, whilst the numerical results presented below concern the true rectangular corrugation.

For numerical calculations we used the following values: $R^{out} = 0.4$ m, $H = 0.003$ m, $R_{in} = 0.01$ m, $l = 0.05$ m, $H(a_1+a_2) = 0.005$ m, $y^* l = 0.045$ m. Then the dimensionless flow parameters are: $\omega = 0.0075$, $\varepsilon = 0.125$, $y^* = 0.9$, $a_1 = 0.167$, $a_2 = 1.5$. The Reynolds number was fixed at $Re = 1.66$, which corresponds to a case where the inertia effects are not negligible but are within the limits of validity of the quasi-rectangular approximation for wall corrugation. Results of the comparison with numerical data are shown in figure 7.

In figure 7 the pressure derivative at the fracture wall ($z = \varphi(r)$) is shown as a function of the radius. The solid oscillating curve corresponds to the numerical simulation of the Navier–Stokes flow through the corrugated fracture. To make a comparison, two dashed lines are added, which represent the asymptotic solution obtained for two smooth fractures forming the representation mentioned above. The aperture of the fracture described by curve 1 is equal to that of the corrugated fracture

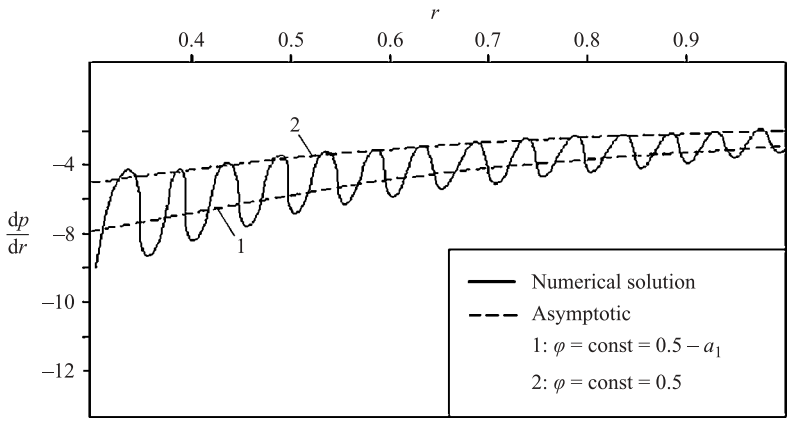

FIGURE 7. Pressure gradient along r: numerical data (undulating curve) and analytical representation formed by the smooth fracture with minimal aperture (curve 1) and the smooth fracture with mean aperture (curve 2).

in the narrowest sections ($\varphi = 1/2 - a_1$). The aperture of the smooth fracture at curve 2 is equal to the mean aperture of the corrugated fracture ($\varphi = 1/2$).

As can be seen, curve 1 smooths the oscillating curve well. From this point of view, the smooth fracture with the aperture equal to the thickness of the narrowest sections can be approximately considered as being the equivalent one.

7. Analysis of the averaged behaviour

7.1. *Macroscale equation of flow*

Double averaging of solution (4.4) in the sense of (3.2) yields the following macroscale flow model through a corrugated radial fracture:

$$\frac{\mathrm{d}}{\mathrm{d}r}\langle\langle p\rangle\rangle = -\frac{3}{2r}\left[\left\langle\frac{1}{\varphi^3}\right\rangle + \frac{2\omega^2}{5\varepsilon^2}\left\langle\frac{\varphi''_{yy}}{\varphi^2} + \frac{(\varphi'_y)^2}{\varphi^3}\right\rangle\right] + \frac{27\omega Re}{70}\frac{1}{r^3}\left\langle\frac{1}{\varphi^2}\right\rangle + \frac{39\omega^2 Re^2}{20790 r^3}\left[\frac{1}{\varepsilon^2}\left\langle\frac{4(\varphi'_y)^2}{\varphi^3} - \frac{3\varphi''_{yy}}{\varphi^2}\right\rangle + \frac{10}{r^2}\left\langle\frac{1}{\varphi}\right\rangle\right], \quad (7.1)$$

$$\langle\langle v\rangle\rangle = 0, \quad \langle\langle u\rangle\rangle = \frac{1}{2r}\left\langle\frac{1}{\varphi}\right\rangle.$$

Equation (7.1) may be rewritten in dimensional form:

$$\frac{\mathrm{d}}{\mathrm{d}R}\langle\langle P\rangle\rangle = -\frac{\mu}{K^{\mathrm{ef}}}\langle\langle U\rangle\rangle + \frac{\rho\beta^{\mathrm{ef}}}{R}\langle\langle U\rangle\rangle^2 + \frac{\rho^2\gamma^{\mathrm{ef}}}{\mu}\langle\langle U\rangle\rangle^3 \quad (7.2)$$

where the three effective parameters K^{ef}, γ^{ef} and β^{ef} are analysed below (see § 7.4, formulae (7.4) and (7.7)).

The averaged equation obtained can be applied to those types of corrugations where the square of the derivative of function $\varphi(y)$ is integrable. In particular, a continuous piecewise differentiable function $\varphi(y)$ satisfies this requirement.

7.2. *Physical meaning of the averaged equation*

First, each term on the right-hand side of (7.1) or (7.2) is in some way subjected to the influence of wall corrugation. However, this influence manifests itself in two different forms. The terms that contain parameter ε are generated by the corrugation, such that in a smooth fracture these terms do not exist. Other terms are non-zero in a smooth case but change their value under the influence of corrugation.

Secondly, it is necessary to distinguish three physical mechanisms that are able to cause an energy or pressure loss: viscous dissipation, the pure inertia effect, and the cross viscous–inertia effect. The pure inertia effect constitutes an irreversible pressure loss due to flow acceleration or deceleration. The cross viscous–inertia effect consists of a supplementary viscous dissipation caused by a deformation of the streamline pattern by the inertia forces.

In a radial fracture the inertia effects have a double origin: the fracture macrogeometry determines a radial deceleration and an averaged velocity variation as $1/R$ ('global inertia effects'), while the wall corrugation determines small-scale oscillations of the velocity vector ('local inertia effects'). The same double origin is appropriate to the cross viscous–inertia terms. The fracture macrogeometry entails a streamline deformation caused by the inertia forces and is described in § 5.1, which is exhibited in the form of a reverse flow. This streamline pattern deformation modifies viscous dissipation, which is called the 'global cross viscous–inertia effect'. The wall corrugation provokes an additional deformation of the streamline pattern, including streamline separation and vortex formation, described in § 6.1. This local streamline deformation is the 'local cross viscous–inertia effect'.

This classification of viscous and inertia effects enables us to explain the physical meaning of the averaged model.

(i) The first term in (7.1) describes the purely viscous dissipation. The main part of this term, which is of order 1, corresponds to the Poiseuille flow in each section (lubrication approximation). The part of order ω^2/ε^2, which, moreover, is proportional to the mean derivative of the corrugation function φ, describes the additional viscous dissipation caused by a more complicated arrangement of the streamlines, especially within the transition zones between the narrow and wide sections.

(ii) The second term, which is of order ωRe, describes the pure inertia effects caused by an irreversible energy loss due to flow acceleration/deceleration. As this term does not contain parameter ε, the averaged inertia effect is 'global', i.e. is caused only by the variation in mean flow velocity along the radius. It does not depend on the derivative φ'_y. Hence it is not zero even in a smooth fracture.

The local pure inertia effect is zero, or in other words, the heterogeneity of the medium geometry (wall corrugation) does not produce the Forchheimer term, quadratic with respect to velocity. This type of disappearance of the pure inertia effects in the averaged model is described in Panfilova, Buès & Panfilov (2002) and Panfilov *et al.* (2003). The reason for this annihilation lies in the fact that the energy loss during flow acceleration or deceleration is not irreversible. The kinetic energy is not lost but is simply transformed into potential energy. If, in addition, the velocity is periodic, then all flow acceleration is balanced by the decelerations, and the total variation in kinetic energy is strictly zero.

(iii) The third term, of order $\omega^2 Re^2/\varepsilon^2$, is the cross viscous–inertia effect. This is an increment of the viscous dissipation caused by a deformation of the streamline pattern, which, in turn, is caused by inertia forces. It contains two parts. The first part is the local cross-term caused by the 'local inertia forces'. It is equal to zero when the

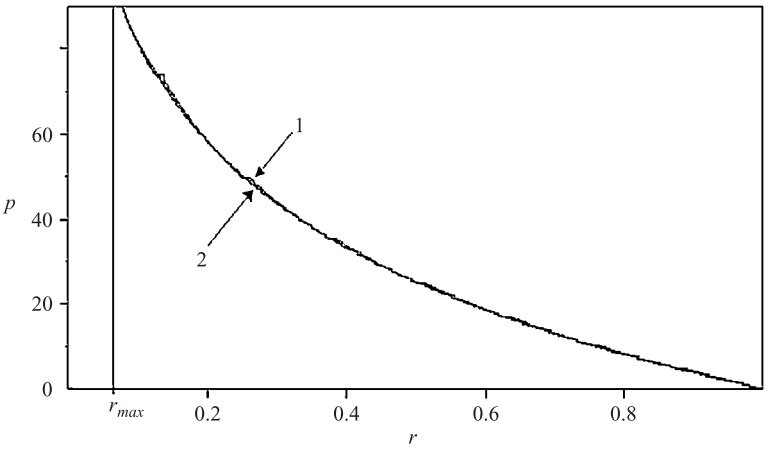

FIGURE 8. Pressure distribution along r: numerical data for pressure averaged over the fracture aperture (curve 1) and analytical twice-averaged pressure (curve 2).

fracture is smooth (the derivative φ'_y is zero). The second part is a result of global inertia forces.

The ratio between the cross inertia–viscous effects and the pure inertia effects is of order $\omega Re\varepsilon^2$. Therefore when $\omega \ll \varepsilon^2$ the pure inertia effect is greater than the cross inertia–viscous effect.

It is important to note that the pure inertia correction to Darcy's law is quadratic with respect to velocity, while the cross inertia–viscous correction is cubic. Therefore, the nonlinear correction in the case of plane-parallel flow is cubic because the global inertia effects are zero in this case.

Stable laminar radial flow in a fracture can be observed for radii greater than r_{max}. Within this domain the asymptotic solution obtained is in good agreement with the numerical data.

7.3. *Comparison of the averaged model with numerical data*

In a particular case of rare corrugation (see § 2.3) when $\omega \ll \varepsilon^2$, the terms of order ω^2/ε^2 can be neglected in (7.1). The first-order approximation with respect to ω is sufficient:

$$\frac{\mathrm{d}}{\mathrm{d}r}\langle\langle p\rangle\rangle = -\frac{3\gamma}{2r}\left\langle\frac{1}{\varphi^3}\right\rangle + \frac{27\omega Re}{70r^3}\left\langle\frac{1}{\varphi^2}\right\rangle. \tag{7.3}$$

This truncated model enables us to describe even the discontinuous function $\varphi(y)$ and the rectangular corrugation in particular.

In figure 8 the twice-averaged pressure (curve 2), calculated based on (3.2) for $Re = 1.66$, is compared with the numerical pressure distribution averaged over z (curve 1). Within the limits of the stable flow ($r \geqslant r_{max}$) the theoretical results fit the numerical data well.

7.4. *Effective fracture permeability*

For a very slow movement, when it is possible for the terms of order Re and higher to be neglected in (7.1), the macroscale model corresponds to Darcy's law:

$$\frac{\mathrm{d}}{\mathrm{d}R}\langle\langle P\rangle\rangle = -\frac{\mu}{K^{\mathrm{ef}}}\langle\langle U\rangle\rangle$$

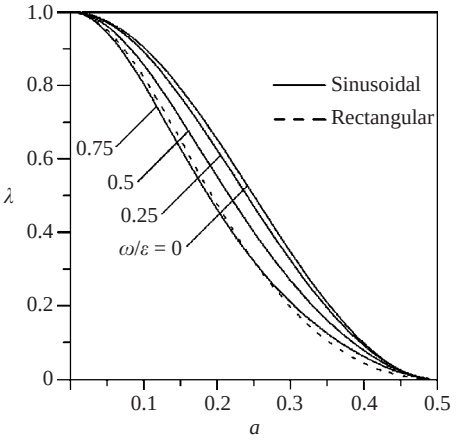

FIGURE 9. Corrugation parameter versus oscillation amplitude for a sinusoidal (solid line) and a rectangular (dashed line) corrugation.

written in dimensional form, where P and U are dimensional pressure and velocity. The effective permeability is defined as

$$K^{\mathrm{ef}} = \frac{H^2}{12}\lambda, \qquad \lambda = \frac{4\left\langle \dfrac{1}{\varphi} \right\rangle}{\left\langle \dfrac{1}{\varphi^3} \right\rangle + \dfrac{2}{5}\left(\dfrac{\omega}{\varepsilon}\right)^2 \left\langle \dfrac{\varphi''_{yy}}{\varphi^2} + \dfrac{(\varphi'_y)^2}{\varphi^3} \right\rangle}. \tag{7.4}$$

Corrugation parameter λ is a correction to the effective permeability caused by wall oscillations. If the fracture is smooth then $\lambda = 1$. For a corrugated fracture, this parameter depends on corrugation amplitude a, wavelength ε, fracture aperture ω and corrugation geometry.

This parameter has been calculated for two types of corrugation: sinusoidal given by function (6.1) and rectangular defined as

$$\varphi = \begin{cases} 0.5(1-a) \text{ when } 0 < y \leqslant 0.5 \\ 0.5(1+a) \text{ when } 0.5 < y \leqslant 1, \quad y = r/\varepsilon. \end{cases} \tag{7.5}$$

Strictly speaking, the quasi-rectangular approximation as in § 6.3 was used, such that the wall discontinuity points were ignored. So λ for a quasi-rectangular corrugation is defined as

$$\lambda \approx 4\left\langle \frac{1}{\varphi} \right\rangle \Big/ \left\langle \frac{1}{\varphi^3} \right\rangle.$$

The integration can be performed in an explicit way; then

$$\lambda \approx \frac{(1-4a^2)^2}{1+12a^2}. \tag{7.6}$$

As shown in (7.4), corrugation parameter λ depends on amplitude a and ratio ω/ε. The dependence of λ on amplitude a is illustrated by figure 9.

It is seen that function λ versus a displays a rather universal behaviour which has a small dependence on corrugation geometry and other parameters. Thus the analytical formula (7.6) may be suggested as a universal model for the corrugation parameter.

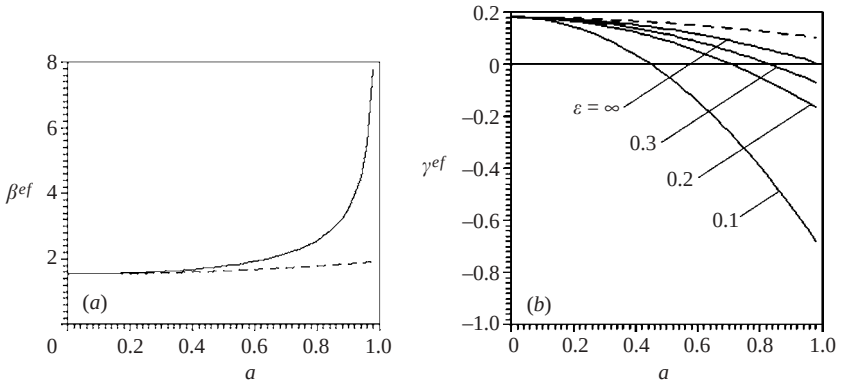

FIGURE 10. (*a*) Inertia parameter β^{ef} and (*b*) inertia–viscous parameter γ^{ef} versus corrugation amplitude a in a quasi-rectangular case (dashed lines) and sinusoidal case (solid lines).

7.5. *Effective inertia and inertia–viscous parameters*

Two new dimensionless parameters appear in (7.2):

$$\beta^{\mathrm{ef}} = \frac{54\left\langle \frac{1}{\varphi^2}\right\rangle}{35\left\langle \frac{1}{\varphi}\right\rangle^2}, \qquad \gamma^{\mathrm{ef}} = \frac{156\omega^2}{13475}\left[\frac{10}{r^2}\frac{1}{\left\langle \frac{1}{\varphi}\right\rangle^2} + \frac{1}{\varepsilon^2}\frac{\left\langle 4\frac{(\varphi_y')^2}{\varphi^3} - 3\frac{\varphi_{yy}''}{\varphi^2}\right\rangle}{\left\langle \frac{1}{\varphi}\right\rangle^3}\right]. \tag{7.7}$$

Parameter β^{ef} represents a specific pressure drop along a unit length caused by the pure inertia effect. Parameter γ^{ef} represents a specific pressure drop along a unit length caused by the cross inertia–viscous phenomena.

Figures 10(*a*) and 10(*b*) illustrate the behaviour of these parameters with respect to corrugation amplitude a for a quasi-rectangular corrugation (dashed lines) and sinusoidal (solid lines). If the corrugation amplitude is not very high, β^{ef} depends on the amplitude only and is the same for the rectangular or for a sinusoidal surface. Thus for $a < 0.6$ the inertia parameter β^{ef}, independently of corrugation geometry, may be calculated by the analytical formula resulting from the quasi-rectangular case:

$$\beta^{\mathrm{ef}} = \frac{54}{35}(1+a^2).$$

In the case of γ^{ef}, the quasi-rectangular approximation is not valid, as seen in figure 10(*b*). However this relation can be used as a basis to develop a good semi-empirical correlation. The following high-precision approximation was found:

$$\left\langle 4\frac{(\varphi_y')^2}{\varphi^3} - 3\frac{\varphi_{yy}''}{\varphi^2}\right\rangle \Big/ \left\langle \frac{1}{\varphi}\right\rangle^3 = -9.9a^2.$$

The following, in practice exact, relation can thus be used to calculate γ^{ef} for any corrugation geometry:

$$\gamma^{\mathrm{ef}} = \frac{156\omega^2}{13475}\left[\frac{5}{2r^2}\left(1-a^2\right)^2 - \frac{9.9}{\varepsilon^2}a^2\right]. \tag{7.8}$$

7.6. Negative inertia–viscous dissipation increment

In (7.8), the left-hand term in the square brackets is responsible for the global inertia–viscous effect, with the same meaning as § 7.2, whereas the right-hand term is caused by the local phenomena. As has been seen, the sign of these terms is opposite. This means that the global streamline deformation by inertia forces always increases the total viscous dissipation, whereas the local streamline deformation is such that total viscous dissipation decreases. Indeed, the inertia forces tend, first, to straighten the streamlines and to reduce the friction trajectory of each liquid particle. The viscous dissipation should therefore decrease.

This general tendency can however be significantly modified by the formation of secondary flows. In the case of global inertia forces, they generate a narrow near-wall zone of secondary flow, which is opposite to the main jet. The friction of a jet against a surface moving in the opposite direction is higher than the friction against a fixed or non-moving surface. As a result, total viscous dissipation increases.

In a slot with corrugated walls, the reverse jets exist in a rather narrow interval of the Reynolds numbers, rapidly being suppressed by local secondary flows. The structure of a local secondary flow is strongly distinct: this is a vortex formed in a zone behind the separation jet. It is well known that a vortex makes practically no contribution to the total viscous dissipation, as the flow velocity therein is very small. These zones may be considered as stagnant. Thus, the local secondary flow cannot reverse the viscous dissipation decrease.

For a high amplitude of wall corrugation, the local inertia forces become somewhat greater than global inertia. Therefore the total viscous dissipation decreases and the inertia–viscous parameter becomes negative. Note that the negative viscous–inertia dissipation increment is equivalent to a reduction in effective permeability.

8. Conclusions

For a radial, steady-state Navier–Stokes flow in a thin cylindrical fracture with periodically corrugated walls, the asymptotic analytical solution is obtained in the limit $\omega \to 0$, where ω is the mean fracture aperture. The case of a 'rare' corrugation is only examined when the fracture aperture is much smaller than the corrugation period. This solution is shown to be in good agreement with the numerical simulation for the Navier–Stokes equations, as in the case of a smooth fracture, as well as in the case of a fracture with a rectangular corrugation which is characterized by a discontinuous function describing the corrugation form. In particular, the solution obtained describes the secondary flow formation and provides rigorous criteria for the appearance of these phenomena.

The macroscopic flow equation is derived by averaging the asymptotic solution both over the fracture aperture and over the wall corrugation. This equation represents a generalized Darcy's law, including two additional nonlinear terms, quadratic and cubic with respect to the mean flow velocity. The quadratic term describes the pure inertia effect, caused by an irreversible loss of kinetic energy due to flow acceleration. The cubic term corresponds to a cross inertia–viscous effect, which consists of an additive viscous dissipation caused by the streamline deformation due to inertia forces.

The inertia–viscous term has a double internal structure, as the streamlines are deformed by inertia forces with two distinct physical origins: 'global forces' caused only by the radial macro-geometry of the domain, and 'local forces' caused only by the wall oscillations. The global forces cause the deformation of a Poiseuille velocity profile until the appearance of a reverse flow in the near-wall domain. The local

inertia forces produce an additional streamline deformation including the effects of flow separation and vortex formation.

In contrast, the pure inertia term is caused only by the global inertia forces. The averaged action of the local inertia forces is zero. The explanation of this effect is suggested in § 7.2.

The suggested macroscale model is characterized by three effective parameters: fracture permeability, the pure inertia parameter and the cross inertia–viscous parameter. All the parameters are a function of the corrugation amplitude and the ratio between the fracture aperture and corrugation length. These functions are calculated for a rectangular and a sinusoidal corrugation. Some approximate analytical formulae were obtained to calculate the effective parameters based on the quasi-rectangular approximation for wall corrugation.

As the inertia forces tend to straighten the flow streamlines, reducing the viscous dissipation, the inertia–viscous parameter should be negative. However, the formation of secondary flows, such as reverse jets, may invert this tendency and may thus change the sign of the inertia–viscous parameter.

REFERENCES

Adler, P. M. & Thovert, J.-F. 1999 *Fractures and Fracture Network*. Kluwer.

Chen, C. 1966 Contribution à l'étude expérimentale de l'écoulement radial d'un fluide visqueux incompressible entre deux disques parallèles. *J. Méc.* **5**, 245–259.

Crosnier, S., Chevalier, S. & Buès, M. 2000 Comparison between numerical simulations and experimental investigations of radial flows in rough fracture. *Advances in Fluid Mechanics III* (ed. M. Ralman & C. A. Brebbia), pp. 43–52. WIT Press.

Iwai, K. 1976 Fundamental studies of fluid flow through a single fracture. PhD thesis, University of California, Berkeley.

Landau, L. D. & Lifshitz, E. M. 1986 *Hydrodynamics*. Nauka, Moscow.

Panfilov, M., Oltean, C., Panfilova, I. & Buès, M. 2003 Singular nature of nonlinear macroscale effects in high-rate flow through porous media. *C. R. Acad. Sci. Paris* IIb **331**, 41–48.

Panfilova, I., Buès, M. & Panfilov, M. 2002 High-rate flow in porous media: d'Alembert paradox and its solution. In *Poromechanics II* (ed. J.-L. Auriault *et al.*), pp. 521–526. A. A. Balkema.

Peube, J.-L. 1963 Sur l'écoulement radial permanent d'un fluide visqueux incompressible entre deux plans parallèles fixes. *J. Méc.* **11**, 377–395.

Renshaw, C. E. 1995 On the relationship between mechanical and hydraulic apertures in rough-walled fractures, *J. Geophys. Res.* **100**, B12, 629–636.

Savage, S. B. 1963 Laminar radial flow betwen parallel plates. *J. Appl. Mech.* 594–596.

Schlichting, H. 1968 *Boundary-layer Theory*. McGraw-Hill.

Skjetne, E., Hansen, A. & Gudmundsson, J. S. 1999 High velocity flow in a rough fracture. *J. Fluid Mech.* **383**, 1–28.

Vatistas, G. H., Ghila, A. & Zitouni, G. 1995 Radial inflow between two flat disks. *Acta Mechanica* **113**, 109–118.

Zimmerman, R. W. & Bodvarsson, G. S. 1996 Effective transmissivity of two-dimensional fracture networks. *Intl J. Rock Mech. Min. Sci. Geomech. Abstr.* **33**, 433–438.

Zitouni, G. & Vatistas G. H. 1997 Purely accelerating flows within two flat disks. *Acta Mechanica* **123**, 151–161.